

INACCURACIES OF ANISOTROPIC MAGNETO-RESISTANCE ANGLE SENSORS DUE TO ASSEMBLY TOLERANCES

U. Ausserlechner*

Infineon Technologies Austria AG, Siemensstrasse 2, 9500 Villach, Austria

Abstract—A large class of angle sensors uses a small permanent magnet attached to the rotor. The magnet is polarized perpendicularly to the axis of rotation, and a magnetic field sensor is placed ahead on the axis. The sensor circuit consists of two full bridges at 45° , each having four anisotropic magneto-resistive (AMR) elements. Even though the electronic system may be calibrated to have nearly no errors like offset, nonlinearity, and mismatch, still significant angle errors may result from assembly tolerances of the magnet and the sensor. This work gives an analytical description of the angle error caused by tilts and eccentricities of magnet and sensor elements against the axis of rotation. Particular emphasis is given to worst case combinations of all tolerances. One part of the angle error can be cancelled by an optimized layout of the AMR-resistors. The remaining part is identical to the case of giant magneto-resistive (GMR) angle sensors. Errors of both AMR and GMR angle sensors are effectively reduced by identical optimization of the shape of magnets. One such optimized shape is disclosed.

1. INTRODUCTION

Magnetic angle sensors consist of a small permanent magnet on a rotating shaft and a magnetic field sensor attached to the stator system (Figure 1). The magnetic field sensor detects the field of the rotating magnet and concludes back on the rotational position of the shaft.

The sensor element is usually a Hall effect device or a magneto-resistive device [1]. Here we focus on anisotropic magneto-resistors (AMR) [2–7].

Received 28 February 2012, Accepted 27 March 2012, Scheduled 5 April 2012

* Corresponding author: Udo Ausserlechner (udo.ausserlechner@infineon.com).

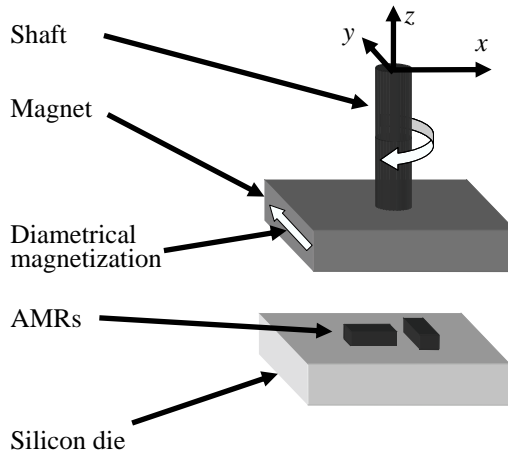


Figure 1. Angle sensor with sensor die placed below a magnet attached to the end of a rotating shaft. Anisotropic magneto-resistors are on top of a silicon die. Only two AMR strips are shown representative of all 8 strips. The straight white arrow denotes the direction of the dipole moment of the magnet.

Angle errors are partly caused by the sensor elements, partly by the electronic processing, and partly by assembly tolerances of the system. Fortunately sensor technology, electronic circuits, and automated calibration in the end-of-line test of the semiconductor manufacturers are continuously improving. Therefore the accuracy of future systems will be dominated by assembly tolerances. In preceding works the author explained how assembly tolerances of giant magneto-resistive (GMR) sensors give rise to angle errors [8, 9]. This paper derives analogous and even more general results for AMR sensors. It shows that the conditions for optimum magnets and optimum layouts are identical for AMR and GMR sensors. One essential conclusion is that for optimum layouts assembly tolerances give rise to identical angle errors for AMR and GMR sensors.

The paper starts by the definition of the required symmetry properties of the magnet. Then we describe all assembly tolerances considered. The operation principle of an angle sensor with two full bridges (= 8 AMR elements) is sketched. Then the essential Equations (19)–(21) for the angle error are derived. Finite size effects of the AMR-elements are described by an additional term Λ^{AMR} , a discussion of which leads to general layout rules for optimum AMR-elements. An approximation for the maximum angle error is derived,

where all assembly tolerances add up in a worst case combination. Finally, plots of angle error versus size of magnet are given and an optimized magnet geometry is disclosed. All definitions and symbols used are consistent with the preceding papers [8, 9].

2. SYMMETRY REQUIREMENTS FOR THE MAGNET

We use a right-handed coordinate system (x, y, z) with orthogonal unit vectors $\vec{n}_x, \vec{n}_y, \vec{n}_z$. The magnet may have the shape of a block, a bar, a cylinder, a tablet, a sphere, or a ring. In general it only has to be symmetrical to the planes $x = 0$ and $y = 0$. Its dipole moment is parallel to the y -direction, yet, the magnetization is not necessarily homogenous. The symmetry leads to the following constraints: the x - and z -components of the magnetic field vanish in the plane $y = 0$: $B_x(x, 0, z) = 0, B_z(x, 0, z) = 0$. Also, the gradient of the y -component orthogonal to this plane vanishes: $\partial B_y(x, 0, z)/\partial y = 0$. Therefore all higher derivatives of these quantities with respect to x and z vanish there, too. Moreover, the slope of the y -component of the magnetic field with respect to x -direction vanishes everywhere on the z -axis: $\partial B_y(0, 0, z)/\partial x = 0$.

3. ASSEMBLY TOLERANCES

In general the magnet is mounted slightly eccentrically to the shaft. We describe this with a translation of the coordinate system: $x^{(1)} = x - \delta_x, y^{(1)} = y - \delta_y, z^{(1)} = z - \delta_z$ with unit vectors $\vec{n}_x^{(1)} = \vec{n}_x, \vec{n}_y^{(1)} = \vec{n}_y, \vec{n}_z^{(1)} = \vec{n}_z$. The origin $x^{(1)} = y^{(1)} = z^{(1)} = 0$ lies on the axis of rotation. Next the magnetization[†] of the magnet may be twisted out of the $y^{(1)}$ -axis by an angle α (rotated around the $z^{(1)}$ -axis). This rotation is described by a unitary rotation matrix $R_z(\alpha)$ [10]

$$\begin{pmatrix} x^{(2)} \\ y^{(2)} \\ z^{(2)} \end{pmatrix} = R_z(\alpha) \begin{pmatrix} x^{(1)} \\ y^{(1)} \\ z^{(1)} \end{pmatrix}, \quad \begin{pmatrix} \vec{n}_x^{(2)} \\ \vec{n}_y^{(2)} \\ \vec{n}_z^{(2)} \end{pmatrix} = R_z(\alpha) \begin{pmatrix} \vec{n}_x^{(1)} \\ \vec{n}_y^{(1)} \\ \vec{n}_z^{(1)} \end{pmatrix},$$

$$R_z(\alpha) = \begin{pmatrix} \cos \alpha & \sin \alpha & 0 \\ -\sin \alpha & \cos \alpha & 0 \\ 0 & 0 & 1 \end{pmatrix}$$

[†] Note that we defined the direction of magnetization parallel to the y -axis.

Next the magnet is rotated around $y^{(2)}$ -axis by a tilt angle β

$$\begin{pmatrix} x^{(3)} \\ y^{(3)} \\ z^{(3)} \end{pmatrix} = R_y(\beta) \begin{pmatrix} x^{(2)} \\ y^{(2)} \\ z^{(2)} \end{pmatrix}, \quad \begin{pmatrix} \vec{n}_x^{(3)} \\ \vec{n}_y^{(3)} \\ \vec{n}_z^{(3)} \end{pmatrix} = R_y(\beta) \begin{pmatrix} \vec{n}_x^{(2)} \\ \vec{n}_y^{(2)} \\ \vec{n}_z^{(2)} \end{pmatrix},$$

$$R_y(\beta) = \begin{pmatrix} \cos\beta & 0 & -\sin\beta \\ 0 & 1 & 0 \\ \sin\beta & 0 & \cos\beta \end{pmatrix}$$

Finally the rotation of the shaft is described by an angle φ around the $z^{(3)}$ -axis: $R_z(\varphi)$. One may use a single transformation matrix $A(\alpha, \beta, \varphi) = R_z(\varphi) R_y(\beta) R_z(\alpha)$ to sum up all these rotations by $\vec{r}^{(4)} = A(\alpha, \beta, \varphi) \vec{r}^{(1)}$. The coordinate system $(x^{(4)}, y^{(4)}, z^{(4)})$ is fixed in space, while the magnet rotates, and the $z^{(4)}$ -axis is identical to the axis of rotation.

The center of the sensor die is shifted via a translation $x^{(5)} = x^{(4)} - \varepsilon_x$, $y^{(5)} = y^{(4)} - \varepsilon_y$, $z^{(5)} = z^{(4)} - \varepsilon_z$. The sensor die is tilted against the axis of rotation by a general Euler rotation

$$\begin{pmatrix} x^{(5)} \\ y^{(5)} \\ z^{(5)} \end{pmatrix} = A^T(\gamma, \lambda, \vartheta) \begin{pmatrix} x^{(8)} \\ y^{(8)} \\ z^{(8)} \end{pmatrix}, \quad \begin{pmatrix} \vec{n}_x^{(5)} \\ \vec{n}_y^{(5)} \\ \vec{n}_z^{(5)} \end{pmatrix} = A^T(\gamma, \lambda, \vartheta) \begin{pmatrix} \vec{n}_x^{(8)} \\ \vec{n}_y^{(8)} \\ \vec{n}_z^{(8)} \end{pmatrix}$$

The first rotation is around the $z^{(4)}$ -axis by the angle γ , the second around the $y^{(5)}$ -axis is the tilt λ between the rotation axis and the normal vector of the die surface, and the last one is a rotation ϑ in the plane of the die surface. For small misalignments β , λ , ϑ are small angles while α and γ are uniformly distributed in $[0^\circ, 180^\circ]$. The rotation angle φ takes on values between 0° and 180° for simple AMR angle sensors. Advanced sensors may detect an entire revolution so that we keep $0^\circ \leq \varphi < 360^\circ$. This is compatible with [8, 9].

With these transformations we can express x , y , z , \vec{n}_x , \vec{n}_y , \vec{n}_z in terms of the coordinates of the sensor die $x^{(8)}$, $y^{(8)}$, $z^{(8)}$, $\vec{n}_x^{(8)}$, $\vec{n}_y^{(8)}$, $\vec{n}_z^{(8)}$ and vice versa. $\vec{n}_x^{(8)}$, $\vec{n}_y^{(8)}$ lie in the die surface and $\vec{n}_z^{(8)}$ is perpendicular to it. $x^{(8)}$, $y^{(8)}$ describe the sensor layout, that is the locations of the infinitely small AMR-sensor elements on the die[‡]. The AMR sensors are on top of the die at $z^{(8)} = 0$. The field components $B_x^{(8)}$, $B_y^{(8)}$, $B_z^{(8)}$ in the layout coordinate system are functions of the coordinates in the die surface $x^{(8)}$, $y^{(8)}$ and of all parameters of position tolerances in Table 1.

[‡] At this moment we still consider the sensors point-like — Subsection 4.2 expands this theory to sensors with finite size.

Table 1. Assembly tolerances grouped in translational tolerances $\delta_x, \delta_y, \delta_z, \varepsilon_x, \varepsilon_y, \varepsilon_z$, and angular tolerances $\alpha, \beta, \gamma, \lambda, \vartheta$. Types of distribution functions and numerical values of spreads used in the following are given in the last column. Stdev means standard deviation.

Symbol	Description	Range of values
δ_x, δ_y	Eccentricity of the magnet with respect to the axis of rotation	Gaussian distributed: mean = 0, stdev = 0.05 ... 0.2 mm
δ_z	Shift of magnet along the axis of rotation	Gaussian distributed: mean = 0, stdev = 0.05 ... 0.2 mm
$\varepsilon_x, \varepsilon_y$	Eccentricity of sensor die with respect to the axis of rotation	Gaussian distributed: mean = 0, stdev = 0.05 ... 0.2 mm
ε_z	Distance of surface of sensor die to the centre of the magnet	Gaussian distributed: mean = nominal value of a few millimetres, stdev = 0.1 ... 0.3 mm
α	Azimuthal angle, by which the magnet is rotated around its vertical axis before being tilted against the axis of rotation	Uniformly distributed in $[0^\circ, 180^\circ]$
β	Tilt angle of magnet with respect to axis of rotation	Gaussian distributed: mean = 0, stdev = 0.2 ... 1°
φ	Rotation angle = angle of rotation of the mechanical member, which has to be detected	0° ... 180° (simple systems) 0° ... 360° (advanced systems)
γ	Azimuthal angle, by which the sensor is rotated around its vertical axis before being tilted against the axis of rotation	Uniformly distributed in $[0^\circ, 180^\circ]$
λ	Tilt angle of die surface with respect to axis of rotation	Gaussian distributed: mean = 0, stdev = 0.5 ... 2°
ϑ	Angle by which the sensor die is rotated around its vertical axis	Gaussian distributed: mean = 0, stdev = 1°

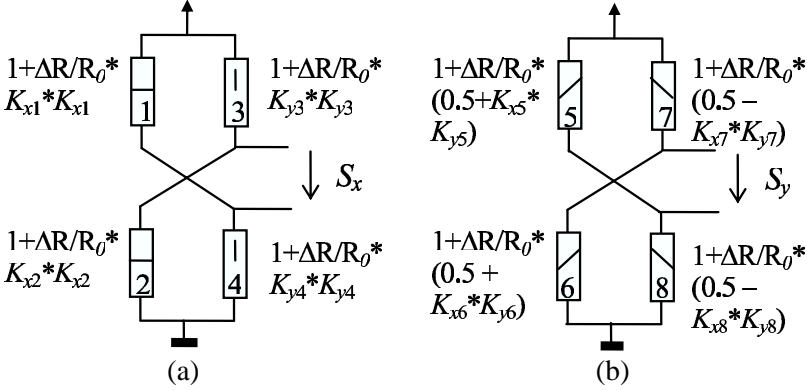


Figure 2. Schematics of the four AMR resistors of a full (a) X-bridge with output signal S_x and (b) Y-bridge with output signal S_y . The lines inside the symbols of the resistors denote the direction of current flow in the AMRs.

4. THE 8-AMR ANGLE SENSOR

4.1. The Operation Principle of the 8-AMR Angle Sensor

The sensor consists of 8 AMR resistors: Four X-AMRs are connected to a full bridge circuit (Figure 2). They are aligned so that the current flows in $x^{(8)}$ - and $y^{(8)}$ -directions. Four Y-AMRs are rotated by 45° against the X-AMRs. The current flow through AMR-resistor 1 is parallel to $x^{(8)}$ -direction. Its resistance is given by $R_1 = R_0 + \Delta R \cos^2 \kappa_1$, where R_0 is a base resistance and ΔR is the maximum resistance change due to AMR-effect (typically 2.5% of base resistance [11]). The angle κ_1 is between the projection of the magnetic field into the die surface (the in-plane field component) and the $x^{(8)}$ -direction

$$\cos \kappa_1 = K_{x,1} = B_x^{(8)}(xx_1, yy_1) / \sqrt{\left(B_x^{(8)}(xx_1, yy_1)\right)^2 + \left(B_y^{(8)}(xx_1, yy_1)\right)^2} \quad (1)$$

with AMR-resistor 1 located at $xx_1 \vec{n}_x^{(8)} + yy_1 \vec{n}_y^{(8)}$. The direction of current through AMR-resistor 3 is parallel to $y^{(8)}$ -direction. Hence, its resistance is given by $R_3 = R_0 + \Delta R \cos^2 (\pi/2 - \kappa_3) = R_0 + \Delta R \sin^2 \kappa_3$. The angle κ_3 is between the in-plane field component and the $x^{(8)}$ -direction on the location of AMR-resistor 3 with

$$\sin \kappa_3 = K_{y,3} = B_y^{(8)}(xx_3, yy_3) / \sqrt{\left(B_x^{(8)}(xx_3, yy_3)\right)^2 + \left(B_y^{(8)}(xx_3, yy_3)\right)^2} \quad (2)$$

AMR-resistor 5 is parallel to $\vec{n}_x^{(8)} + \vec{n}_y^{(8)}$. Its resistance is $R_5 = R_0 + \Delta R (0.5 + K_{x,5}K_{y,5})$. AMR-resistor 7 is parallel to $\vec{n}_x^{(8)} - \vec{n}_y^{(8)}$. Its resistance is $R_7 = R_0 + \Delta R (0.5 - K_{x,7}K_{y,7})$.

For 1 V supply voltage of both bridges and $\Delta R \ll R_0$ the output voltages are

$$S_x \cong \sigma (\Delta R / (4R_0)) (K_{x,1}^2 + K_{x,2}^2 - K_{y,3}^2 - K_{y,4}^2) \quad (3)$$

$$S_y \cong \sigma (\Delta R / (4R_0)) (K_{x,5}K_{y,5} + K_{x,6}K_{y,6} + K_{x,7}K_{y,7} + K_{x,8}K_{y,8}) \quad (4)$$

$\sigma = 1$ if the dipole moment of the magnet points in negative y -direction. $\sigma = -1$ if the dipole moment of the magnet points in positive y -direction. Some AMR angle sensors use only half-bridges instead of full bridges like in Figure 2. Thus they need only four instead of eight AMR resistors. In this case half of the terms in (3), (4) have to be dismissed.

For vanishing assembly tolerances ($\beta = \lambda = \delta_x = \delta_y = \varepsilon_x = \varepsilon_y = 0$) and point-like AMRs this gives

$$S_x \cong -(\Delta R / (2R_0)) \cos(2\alpha + 2\gamma + 2\varphi + 2\vartheta),$$

$$S_y \cong (\Delta R / (2R_0)) \sin(2\alpha + 2\gamma + 2\varphi + 2\vartheta)$$

The signal S_x is the signal of the X-channel or cosine-channel whereas the signal S_y is the signal of the Y-channel or sine-channel[§]. The sensor estimates the rotation angle by

$$\tan(2\alpha + 2\gamma + 2\varphi' + 2\vartheta) = -S_y / S_x. \quad (5)$$

φ' is the estimated angle, φ is the true angle of rotation, and the difference is the delta-angle $\Delta\varphi = \varphi - \varphi'$.

$$\tan(2\Delta\varphi) = \frac{S_x \tan(2\alpha + 2\gamma + 2\varphi + 2\vartheta) + S_y}{S_x - S_y \tan(2\alpha + 2\gamma + 2\varphi + 2\vartheta)} \quad (6)$$

As global measures of the angle error we define

$$AE = \frac{1}{2} \left(\max_{\varphi \in [0^\circ \dots 360^\circ]} \Delta\varphi - \min_{\varphi \in [0^\circ \dots 360^\circ]} \Delta\varphi \right) \quad (7)$$

$$ME = \max \left\{ \left| \max_{\varphi \in [0^\circ \dots 360^\circ]} \Delta\varphi \right|, \left| \min_{\varphi \in [0^\circ \dots 360^\circ]} \Delta\varphi \right| \right\}. \quad (8)$$

ME denotes the largest deviation between measured angle and true angle whereas AE is half of the width of an error band around an optimum center value. AE specifies the nonlinearity of the angle sensor similar to the INL (= integral non-linearity) for analog-to-digital converters.

[§] Swap sine- and cosine-channels if the magnetization of the magnet points into x - instead of y -axis.

4.2. The Finite Size of the AMRs

Since AMRs are metallic conductors they have a small sheet resistance. On the other hand integrated circuit designers prefer large resistance values from 1...10kOhm: They can be biased with the full supply voltage in the order of several volts and they still draw acceptably small currents. Therefore the AMR resistances need a large number of squares. Since the width should not be lower than a few microns due to reasons of accuracy in the photolithographic processes the length of the AMRs has to be large (in the order of millimeters). So far the problem is similar to large MOS-transistors in differential input pairs of operational amplifiers or large resistors, which need to match well. There are several layout techniques for this well known problem in integrated circuit design. One popular solution is inter-digital layout where each long device A and B is split up into smaller parts A_1, A_2, \dots and B_1, B_2, \dots and the placement on the die is $A_1-B_1-A_2-B_2-\dots$. Due to this layout technique the centers of gravity of both devices A and B are close to each other and therefore the matching is optimized [12]. This principle can be used for the AMRs in each half-bridge: Both resistances are composed of several strips, which are parallel to each other, yet they have Barber-poles tilted with $+45^\circ$ against the strip length for the one resistance and with -45° for the other resistance. With this method it is possible to make an inter-digital layout for all resistances of the X-bridge and for all resistances of the Y-bridge. However the strips of the Y-bridge are at 45° to the strips of the X-bridge and therefore it is difficult to place them in close proximity. The overall area used by these 8 AMRs is roughly $0.6\text{ mm} \times 0.6\text{ mm}$. It is obvious that the magnetic field of small magnets is not perfectly homogeneous over this large area. Consequently the factors K_x, K_y assume different values as the local coordinates $x^{(8)}, y^{(8)}$ subtend the entire region of the AMR. Consider a strip of AMR of width w and thickness t with electrical resistivity ρ_{el} at zero magnetic field extending from x_{start} to x_{stop} in x -direction. It has the resistance $R'(y^{(8)}) = (\rho_{el}/(tw)) \int_{x_{start}}^{x_{stop}} (1 + (\Delta R/R_0)K_x^2(x^{(8)}, y^{(8)}))dx^{(8)}$. For n meanders between y_{start} and $y_{stop} = y_{start} + n \times w$ the total resistance is $R = (n/(y_{stop} - y_{start})) \int_{y_{start}}^{y_{stop}} R'(y^{(8)})dy^{(8)}$. Hence, the resistance of the i -th AMR meander in an inhomogeneous magnetic field is

$$R_i = R_0 + \Delta R (K_{x,i}^2)_{eff}$$

$$\text{with } (K_{x,i}^2)_{eff} = (1/A_i) \int_{A_i} K_{x,i}^2(x^{(8)}, y^{(8)}) dx^{(8)} dy^{(8)} \quad (9)$$

with $A_i = (x_{stop} - x_{start})(y_{stop} - y_{start})$. Thus one can easily take account of the finite size of the AMRs by using $(K_{x,i}^2)_{eff}, (K_{y,i}^2)_{eff}$,

$(K_{x,i}K_{y,i})_{eff}$ in (3), (4), which are merely averages of K_x^2 , K_y^2 , K_xK_y over the areas covered by the AMR meanders.

4.3. A Taylor Series Expansion for Small Assembly Tolerances

For small assembly tolerances and not too big AMR size we may develop (1) into a Taylor series. For the i -th AMR the lowest order terms are

$$K_{x,i} = \sigma \sin(\alpha + \gamma + \varphi + \vartheta) + \sigma \cos(\alpha + \gamma + \varphi + \vartheta) \sum_{j=1}^{15} C_{ji} p_j, \quad (10)$$

The first term in (10) is the value for point-like i -th AMR and without position tolerances of magnet and sensor. The sum in the second term accounts for all position tolerances and for the finite size of the i -th AMR resistor strip:

$$\begin{aligned} & \sigma \cos(\alpha + \gamma + \varphi + \vartheta) \sum_{j=1}^{15} C_{ji} p_j \\ &= \frac{\partial^2 K_{x,i}}{\partial \beta^2} \frac{\beta^2}{2} + \frac{\partial^2 K_{x,i}}{\partial \delta_r^2} \frac{\delta_r^2}{2} + \frac{\partial^2 K_{x,i}}{\partial \lambda^2} \frac{\lambda^2}{2} + \frac{\partial^2 K_{x,i}}{\partial \varepsilon_r^2} \frac{\varepsilon_r^2}{2} + \frac{\partial^2 K_{x,i}}{\partial r_i^2} \frac{r_i^2}{2} \\ &+ \frac{\partial^2 K_{x,i}}{\partial \beta \partial \lambda} \beta \lambda + \frac{\partial^2 K_{x,i}}{\partial \beta \partial \varepsilon_r} \beta \varepsilon_r + \frac{\partial^2 K_{x,i}}{\partial \beta \partial \delta_r} \beta \delta_r + \frac{\partial^2 K_{x,i}}{\partial \beta \partial r_i} \beta r_i + \frac{\partial^2 K_{x,i}}{\partial \lambda \partial \varepsilon_r} \lambda \varepsilon_r \\ &+ \frac{\partial^2 K_{x,i}}{\partial \lambda \partial \delta_r} \lambda \delta_r + \frac{\partial^2 K_{x,i}}{\partial \lambda \partial r_i} \lambda r_i + \frac{\partial^2 K_{x,i}}{\partial \varepsilon_r \partial \delta_r} \varepsilon_r \delta_r + \frac{\partial^2 K_{x,i}}{\partial \varepsilon_r \partial r_i} \varepsilon_r r_i + \frac{\partial^2 K_{x,i}}{\partial \delta_r \partial r_i} \delta_r r_i \end{aligned} \quad (11)$$

In (11) the eccentricities and the position coordinates of the i -th AMR were re-written in cylindrical coordinates $\delta_x = \delta_r \cos \eta$, $\delta_y = \delta_r \sin \eta$, $\varepsilon_x = \varepsilon_r \cos \chi$, $\varepsilon_y = \varepsilon_r \sin \chi$, $xx_i = r_i \cos \omega_i$, $yy_i = r_i \sin \omega_i$. AMRs 3 and 4 need a similar Taylor series for K_y of (2) with

$$K_{y,i} = \sigma \cos(\alpha + \gamma + \varphi + \vartheta) - \sigma \sin(\alpha + \gamma + \varphi + \vartheta) \sum_{j=1}^{15} C_{ji} p_j, \quad (12)$$

The definitions of K_x in (1) and K_y in (2) are identical to (9a, b) in [8] and (5a, b) in [9]. Therefore we can use the expressions (18a-j) in [8] and (17a-e) in [9] for the derivatives in (11). This gives

$$\begin{aligned} C_{1,i} p_1 &= \frac{\partial^2 K_x}{\partial \beta^2} \frac{\sigma \beta^2}{2 \cos(\alpha + \gamma + \varphi + \vartheta)} = \frac{\beta^2}{4} \sin(2\alpha) \left\{ 2\varepsilon_z (\varepsilon_z \tilde{E} - \tilde{T}) - 1 \right\} \\ C_{2,i} p_2 &= \frac{\partial^2 K_x}{\partial \delta_r^2} \frac{\sigma \delta_r^2}{2 \cos(\alpha + \gamma + \varphi + \vartheta)} = \frac{\delta_r^2}{2} \sin(2\eta) \tilde{E} \end{aligned}$$

$$\begin{aligned}
C_{3,i}p_3 &= \frac{\partial^2 K_x}{\partial \lambda^2} \frac{\sigma \lambda^2}{2 \cos(\alpha + \gamma + \varphi + \vartheta)} = -\frac{\lambda^2}{4} \sin(2\alpha + 2\gamma + 2\varphi) \\
C_{4,i}p_4 &= \frac{\partial^2 K_x}{\partial \varepsilon_r^2} \frac{\sigma \varepsilon_r^2}{2 \cos(\alpha + \gamma + \varphi + \vartheta)} = \frac{\varepsilon_r^2}{2} \tilde{E} \sin(2\alpha + 2\chi + 2\varphi) \\
C_{5,i}p_5 &= \frac{\partial^2 K_x}{\partial r_i^2} \frac{\sigma r_i^2}{2 \cos(\alpha + \gamma + \varphi + \vartheta)} \\
&= (r_i^2/2) \tilde{E} \sin(2\alpha + 2\gamma + 2\varphi + 2\vartheta + 2\omega_i) \\
C_{6,i}p_6 &= \frac{\partial^2 K_x}{\partial \beta \partial \lambda} \frac{\sigma \beta \lambda}{\cos(\alpha + \gamma + \varphi + \vartheta)} = -\beta \lambda \cos(\alpha + \gamma + \varphi) \sin \alpha \left(\varepsilon_z \tilde{T} + 1 \right) \\
C_{7,i}p_7 &= \frac{\partial^2 K_x}{\partial \beta \partial \varepsilon_r} \frac{\sigma \beta \varepsilon_r}{\cos(\alpha + \gamma + \varphi + \vartheta)} \\
&= \beta \varepsilon_r \left\{ \varepsilon_z \tilde{E} \sin(2\alpha + \chi + \varphi) - \tilde{T} \cos \alpha \sin(\alpha + \chi + \varphi) \right\} \\
C_{8,i}p_8 &= \frac{\partial^2 K_x}{\partial \beta \partial \delta_r} \frac{\sigma \beta \delta_r}{\cos(\alpha + \gamma + \varphi + \vartheta)} = \beta \delta_r \left\{ \varepsilon_z \tilde{E} \sin(\alpha + \eta) - \tilde{T} \cos \alpha \sin \eta \right\} \\
C_{9,i}p_9 &= \frac{\partial^2 K_x}{\partial \beta \partial r_i} \frac{\sigma \beta r_i}{\cos(\alpha + \gamma + \varphi + \vartheta)} \\
&= \beta r_i \left\{ \varepsilon_z \tilde{E} \sin(2\alpha + \gamma + \varphi + \vartheta + \omega_i) \right. \\
&\quad \left. - \tilde{T} \cos \alpha \sin(\alpha + \gamma + \varphi + \vartheta + \omega_i) \right\} \\
C_{10,i}p_{10} &= \frac{\partial^2 K_x}{\partial \lambda \partial \varepsilon_r} \frac{\sigma \lambda \varepsilon_r}{\cos(\alpha + \gamma + \varphi + \vartheta)} = -\lambda \varepsilon_r \cos(\alpha + \gamma + \varphi) \sin(\alpha + \chi + \varphi) \tilde{T} \\
C_{11,i}p_{11} &= \frac{\partial^2 K_x}{\partial \lambda \partial \delta_r} \frac{\sigma \lambda \delta_r}{\cos(\alpha + \gamma + \varphi + \vartheta)} = -\lambda \delta_r \cos(\alpha + \gamma + \varphi) \sin \eta \tilde{T} \\
C_{12,i}p_{12} &= \frac{\partial^2 K_x}{\partial \lambda \partial r_i} \frac{\sigma \lambda r_i}{\cos(\alpha + \gamma + \varphi + \vartheta)} \\
&= -\lambda r_i \tilde{T} \cos(\alpha + \gamma + \varphi) \sin(\alpha + \gamma + \varphi + \vartheta + \omega_i) \\
C_{13,i}p_{13} &= \frac{\partial^2 K_x}{\partial \varepsilon_r \partial \delta_r} \frac{\sigma \varepsilon_r \delta_r}{\cos(\alpha + \gamma + \varphi + \vartheta)} = \varepsilon_r \delta_r \tilde{E} \sin(\alpha + \chi + \eta + \varphi) \\
C_{14,i}p_{14} &= \frac{\partial^2 K_x}{\partial \varepsilon_r \partial r_i} \frac{\sigma \varepsilon_r r_i}{\cos(\alpha + \gamma + \varphi + \vartheta)} = \varepsilon_r r_i \tilde{E} \sin(2\alpha + \chi + \gamma + 2\varphi + \vartheta + \omega_i) \\
C_{15,i}p_{15} &= \frac{\partial^2 K_x}{\partial \delta_r \partial r_i} \frac{\sigma \delta_r r_i}{\cos(\alpha + \gamma + \varphi + \vartheta)} = \delta_r r_i \tilde{E} \sin(\alpha + \eta + \gamma + \varphi + \vartheta + \omega_i)
\end{aligned}$$

with $\tilde{E} = \partial^2 B_x(0, 0, \varepsilon_z + \delta_z) / \partial x / \partial y / B_y(0, 0, \varepsilon_z + \delta_z)$ and $\tilde{T} = \partial B_z(0, 0, \varepsilon_z + \delta_z) / \partial y / B_y(0, 0, \varepsilon_z + \delta_z)$. Note that these functions \tilde{E}, \tilde{T} are slightly different from the shape functions E, T in [8, 9]: $\tilde{E} = \sigma E, \tilde{T} = -\sigma T$. They are both computed in the coordinate system (x, y, z) fixed to the magnet.

From (10) and (12) we obtain the following terms

$$K_{x,i}^2 \cong \sin^2(\alpha + \gamma + \varphi + \vartheta) + \sin(2\alpha + 2\gamma + 2\varphi + 2\vartheta) \sum_{j=1}^{15} C_{ji} p_j \quad (13)$$

$$K_{y,i}^2 \cong \cos^2(\alpha + \gamma + \varphi + \vartheta) - \sin(2\alpha + 2\gamma + 2\varphi + 2\vartheta) \sum_{j=1}^{15} C_{ji} p_j \quad (14)$$

$$K_{x,i} K_{y,i} \cong 0.5 \sin(2\alpha + 2\gamma + 2\varphi + 2\vartheta) + \cos(2\alpha + 2\gamma + 2\varphi + 2\vartheta) \sum_{j=1}^{15} C_{ji} p_j \quad (15)$$

where we neglected the squares of the sums, because they are small of higher order.

In order to account for the finite size of the AMR elements we have to compute the average of (13)–(15) over the area A_i subtended by the i -th AMR. Only 5 of the 15 terms $C_{ji} p_j$ depend on the location of the test point: 4 of these 5 terms $C_{9,i} p_9, C_{12,i} p_{12}, C_{14,i} p_{14}, C_{15,i} p_{15}$ are linearly dependent of r_i whereas $C_{5,i} p_5$ depends on the square of r_i . With $xx_i = r_i \cos \omega_i$ and $yy_i = r_i \sin \omega_i$ we obtain

$$C_{14,i} p_{14} = \varepsilon_r \tilde{E} (\sin(2\alpha + \chi + \gamma + 2\varphi + \vartheta) xx_i + \cos(2\alpha + \chi + \gamma + 2\varphi + \vartheta) yy_i)$$

The average over the area A_i is

$$(1/A_i) \int_{A_i} C_{14,i} p_{14} dA = \varepsilon_r \tilde{E} (\sin(2\alpha + \chi + \gamma + 2\varphi + \vartheta) \bar{x}_i + \cos(2\alpha + \chi + \gamma + 2\varphi + \vartheta) \bar{y}_i)$$

with the coordinates of the center of gravity $\bar{x}_i = (1/A_i) \int_{A_i} xx_i dA$ and $\bar{y}_i = (1/A_i) \int_{A_i} yy_i dA$. Similar results are obtained for the other linear terms in r_i . Only the term proportional to the square of r_i gives a different result:

$$C_{5,i} p_5 = \tilde{E} \{0.5 (xx_i^2 - yy_i^2) \sin(2\alpha + 2\gamma + 2\varphi + 2\vartheta) + xx_i yy_i \cos(2\alpha + 2\gamma + 2\varphi + 2\vartheta)\}$$

The average over the area A_i is

$$(1/A_i) \int_{A_i} C_{5,i} p_5 dA = \tilde{E} \{0.5 (I_{xx,i} - I_{yy,i}) \sin(2\alpha + 2\gamma + 2\varphi + 2\vartheta) + I_{xy,i} \cos(2\alpha + 2\gamma + 2\varphi + 2\vartheta)\}$$

Here we used the moments of inertia $I_{xx,i} = (1/A_i) \int_{A_i} xx_i^2 dA$ and $I_{yy,i} = (1/A_i) \int_{A_i} yy_i^2 dA$, and the geometrical deviation moment $I_{xy,i} = (1/A_i) \int_{A_i} xx_i yy_i dA$.

4.4. A Closed Form Expression for the Angle Error

Introducing (13)–(15) into (3), (4) leads to

$$S_x \cong \frac{\Delta R}{4R_0} \left(-2 \cos(2\alpha + 2\gamma + 2\varphi + 2\vartheta) + \sin(2\alpha + 2\gamma + 2\varphi + 2\vartheta) \sum_{i=1}^4 \sum_{j=1}^{15} C_{ji} p_j \right) \quad (16)$$

$$S_y \cong \frac{\Delta R}{4R_0} \left(2 \sin(2\alpha + 2\gamma + 2\varphi + 2\vartheta) + \cos(2\alpha + 2\gamma + 2\varphi + 2\vartheta) \sum_{i=5}^8 \sum_{j=1}^{15} C_{ji} p_j \right) \quad (17)$$

Inserting (16) and (17) into (6) gives

$$\tan 2\Delta\varphi = \frac{\left[\sum_{j=1}^{15} \sum_{i=5}^8 C_{ji} p_j + \sin^2(2\alpha + 2\gamma + 2\varphi + 2\vartheta) \right] \times \sum_{j=1}^{15} p_j \left(\sum_{i=1}^4 C_{ji} - \sum_{i=5}^8 C_{ji} \right)}{\left[-2 + 0.5 \sin(4\alpha + 4\gamma + 4\varphi + 4\vartheta) \right] \times \sum_{j=1}^{15} p_j \left(\sum_{i=1}^4 C_{ji} - \sum_{i=5}^8 C_{ji} \right)} \quad (18)$$

Neglecting higher order terms of all small quantities yields

$$\Delta\varphi \cong \Delta\varphi_{\text{opt}} - \Lambda^{\text{AMR}} \quad (19)$$

The overall delta angle is composed of two parts. The first part describes the angle error of a system where all 8 AMRs are point sized and located in the center of the die $x^{(8)} = y^{(8)} = 0$:

$$\begin{aligned} \Delta\varphi_{\text{opt}} &\cong - \lim_{r_i \rightarrow 0} \sum_{j=1}^{15} C_{ji} p_j \\ &= (\beta/2)^2 \sin(2\alpha) + (\lambda/2)^2 \sin(2\alpha + 2\gamma + 2\varphi) + \lambda\beta \sin\alpha \cos(\alpha + \gamma + \varphi) \\ &\quad - (\delta_y + \varepsilon_r \sin(\alpha + \chi + \varphi) + \beta\varepsilon_z \sin\alpha) \{ \tilde{E}(\delta_x + \varepsilon_r \cos(\alpha + \chi + \varphi) \\ &\quad + \beta\varepsilon_z \cos\alpha) - \tilde{T}(\beta \cos\alpha + \lambda \cos(\alpha + \gamma + \varphi)) \} \end{aligned} \quad (20)$$

The second part takes account of the actual position and size (= layout) of the 8 AMRs. In case of an optimized layout it vanishes:

$$\begin{aligned}
 & \Lambda^{\text{AMR}} \\
 & \cong \sin^2 (2\alpha + 2\gamma + 2\varphi + 2\vartheta) \left\{ -\tilde{T} [\beta \cos \alpha + \lambda \cos (\alpha + \gamma + \varphi)] \right. \\
 & \quad \left[\bar{X}_{1,4} \sin(\alpha + \gamma + \varphi + \vartheta) + \bar{Y}_{1,4} \cos(\alpha + \gamma + \varphi + \vartheta) \right] \\
 & \quad + \tilde{E} [0.5 (\bar{X}\bar{X}_{1,4} - \bar{Y}\bar{Y}_{1,4}) \sin(2\alpha + 2\gamma + 2\varphi + 2\vartheta) \\
 & \quad + \bar{X}\bar{Y}_{1,4} \cos(2\alpha + 2\gamma + 2\varphi + 2\vartheta)] + \beta \varepsilon_z \tilde{E} [\bar{X}_{1,4} \sin (2\alpha + \gamma + \varphi + \vartheta) \\
 & \quad + \bar{Y}_{1,4} \cos(2\alpha + \gamma + \varphi + \vartheta)] + \varepsilon_r \tilde{E} [\bar{X}_{1,4} \sin (2\alpha + \chi + \gamma + 2\varphi + \vartheta) \\
 & \quad + \bar{Y}_{1,4} \cos (2\alpha + \chi + \gamma + 2\varphi + \vartheta)] + \delta_r \tilde{E} [\bar{X}_{1,4} \sin (\alpha + \eta + \gamma + \varphi + \vartheta) \\
 & \quad + \bar{Y}_{1,4} \cos(\alpha + \eta + \gamma + \varphi + \vartheta)] \left. \right\} + \cos^2 (2\alpha + 2\gamma + 2\varphi + 2\vartheta) \\
 & \times \left\{ -\tilde{T} [\beta \cos \alpha + \lambda \cos (\alpha + \gamma + \varphi)] [\bar{X}_{5,8} \sin (\alpha + \gamma + \varphi + \vartheta) \right. \\
 & \quad + \bar{Y}_{5,8} \cos(\alpha + \gamma + \varphi + \vartheta)] + \tilde{E} [0.5 (\bar{X}\bar{X}_{5,8} - \bar{Y}\bar{Y}_{5,8}) \sin(2\alpha + 2\gamma + 2\varphi + 2\vartheta) \\
 & \quad + \bar{X}\bar{Y}_{5,8} \cos (2\alpha + 2\gamma + 2\varphi + 2\vartheta)] + \beta \varepsilon_z \tilde{E} [\bar{X}_{5,8} \sin (2\alpha + \gamma + \varphi + \vartheta) \\
 & \quad + \bar{Y}_{5,8} \cos (2\alpha + \gamma + \varphi + \vartheta)] + \varepsilon_r \tilde{E} [\bar{X}_{5,8} \sin (2\alpha + \chi + \gamma + 2\varphi + \vartheta) \\
 & \quad + \bar{Y}_{5,8} \cos (2\alpha + \chi + \gamma + 2\varphi + \vartheta)] + \delta_r \tilde{E} [\bar{X}_{5,8} \sin (\alpha + \eta + \gamma + \varphi + \vartheta) \\
 & \quad \left. + \bar{Y}_{5,8} \cos (\alpha + \eta + \gamma + \varphi + \vartheta)] \right\} \tag{21}
 \end{aligned}$$

With the abbreviations $\bar{X}_{1,4} = \sum_{i=1}^4 \bar{x}_i/4$, $\bar{X}_{5,8} = \sum_{i=5}^8 \bar{x}_i/4$, $\bar{Y}_{1,4} = \sum_{i=1}^4 \bar{y}_i/4$, $\bar{Y}_{5,8} = \sum_{i=5}^8 \bar{y}_i/4$, $\bar{X}\bar{X}_{1,4} = \sum_{i=1}^4 I_{xx,i}/4$, $\bar{Y}\bar{Y}_{1,4} = \sum_{i=1}^4 I_{yy,i}/4$, $\bar{X}\bar{Y}_{1,4} = \sum_{i=1}^4 I_{xy,i}/4$, $\bar{X}\bar{X}_{5,8} = \sum_{i=5}^8 I_{xx,i}/4$, $\bar{Y}\bar{Y}_{5,8} = \sum_{i=5}^8 I_{yy,i}/4$, $\bar{X}\bar{Y}_{5,8} = \sum_{i=5}^8 I_{xy,i}/4$. Comparison of (20) with (25) in [8] shows that the angle errors caused by assembly tolerances are identical for AMRs and GMRs — at least in case of small or optimized sensor elements, where Λ^{AMR} and Λ^{GMR} vanish. Moreover the same shape functions \tilde{E} and \tilde{T} of magnets show up. Hence, any magnet, which is optimized to keep the influence of assembly tolerances on angle errors of AMRs small, at the same time works well for GMRs, too. In (21) all the terms describing the influence of AMR layout on the angle error are summed up in Λ^{AMR} . Even this term is similar to Λ^{GMR} . In particular the rules for optimized layout are identical:

$$\begin{aligned}
 & \bar{X}_{1,4} = \bar{X}_{5,8} = \bar{Y}_{1,4} = \bar{Y}_{5,8} = \bar{X}\bar{Y}_{1,4} = \bar{X}\bar{Y}_{5,8} \\
 & \quad = \bar{X}\bar{X}_{1,4} - \bar{Y}\bar{Y}_{1,4} = \bar{X}\bar{X}_{5,8} - \bar{Y}\bar{Y}_{5,8} = 0 \tag{22}
 \end{aligned}$$

Commercially available AMR-sensors partially comply to these rules, but there are also some which do not. Note that $\Lambda^{\text{AMR}} = 0$ for magnets with vanishing shape-functions, even if the sensor layout does

not fulfil (22). Therefore layout optimization is less powerful than optimization of the magnet, which also makes several terms in $\Delta\varphi_{\text{opt}}$ vanish (cf. (20)).

5. THE MAXIMUM ANGLE ERROR ME

The delta angle of (20) is a sum over 15 sine-functions with 12 different amplitudes and 15 different phases. The phases consist of various sums over the angles α , γ , φ , η , χ . The delta-angle assumes its maximum ME if all angles α , γ , φ , η , χ are chosen such that the peaks of most sine-functions add up. Therefore we may consider the five sine-functions with the largest amplitudes and choose the angles α , γ , φ , η , χ such that these sine-functions add up. This is always possible if we start with α and γ , because all other angles subtend the complete range $0^\circ \dots 360^\circ$. If the other ten amplitudes are small we have a good guess for ME . At least we can obtain an upper boundary

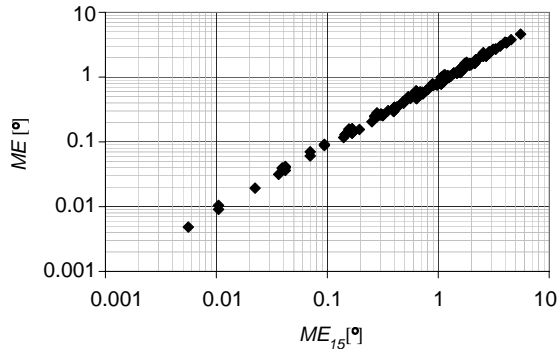


Figure 3. Worst case angle error ME versus ME_{15} of Equation (23) as obtained from numerical simulations for two cylindrical magnets: the first magnet has a diameter of 6 mm, a thickness of 2.5 mm and the sensor is positioned at $\varepsilon_z = -3.6$ mm; the second magnet has a diameter of 10 mm, a thickness of 2 mm and the sensor is positioned at $\varepsilon_z = -2$ mm. 144 combinations of angles β , λ with values 0° , 3° , 6° , 9° and of ε_r , δ_r with values of 0 mm, 0.3 mm, 0.6 mm are tested. For the angles α , η , χ , γ all values in steps of 15° are tested. This gives $12^2 \times 24^2 = 82944 \Delta\varphi_{\text{opt}}$ -curves according to (20) for each of the 144 combinations. For all these $82944 \Delta\varphi_{\text{opt}}$ -curves the ME -angle error is computed according to (8) and the largest value is taken as ordinate in the plot.

for ME (which we call ME_{15}) by adding up all 15 amplitudes:

$$\begin{aligned}
 &ME_{15} \\
 &= (\beta/2)^2 \left| 1 - 2\varepsilon_z \left(\varepsilon_z \tilde{E} - \tilde{T} \right) \right| + (\lambda/2)^2 + \beta\lambda \left| 1 + \varepsilon_z \tilde{T} \right| \\
 &\quad + (\varepsilon_r + \delta_r) \left[(\beta/2) \left(\left| \tilde{T} \right| + \left| 2\varepsilon_z \tilde{E} - \tilde{T} \right| \right) + \lambda \left| \tilde{T} \right| \right] + \left(\left| \tilde{E} \right| / 2 \right) (\varepsilon_r + \delta_r)^2 \quad (23)
 \end{aligned}$$

Comparison with numerical data in Figure 3 shows $ME = ME_{15}/A$ with $A = 1 \dots 1.39$. If some tolerances vanish then also some amplitudes vanish and an appropriate choice for the five angles $\alpha, \gamma, \varphi, \eta, \chi$ can be found such that all other amplitudes add up constructively. This can be accounted for by $A = 1$. In the general case of all assembly tolerances non-vanishing the worst case angle error ME is smaller than ME_{15} so that $A = 1.39$. Figure 4 shows a compilation of data for angle errors due to various combinations of assembly tolerances. If all assembly tolerances are comparably large the ratio of ME_{15}/ME is between 1.13 and 1.34 (1.2 on an average). So in general we may assume that (23) over-estimates the angle error by 20%. On the other hand our whole theory neglects higher order terms in the Taylor Series expansion of the angle error. Therefore we believe that (23) only slightly over-estimates the worst case angle error.

Equation (23) shows that the angle error is more than the sum over individual assembly tolerances: mixed error terms like $\beta\lambda \left| 1 + \varepsilon_z \tilde{T} \right|$,

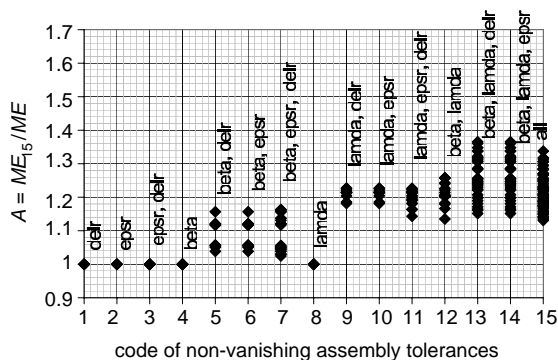


Figure 4. ME_{15}/ME for various combinations of assembly tolerances (same data as in 3): if only single tolerances are present (e.g., only δ_r , only ε_r , only β , only λ like in columns 1, 2, 4, 8 of the plot) $ME_{15} = ME$. However, in practice all assembly tolerances are present: for this case ME_{15}/ME ranges from about 1.1 to about 1.35 (cf. data in column 15), depending on their relative strengths and phase relations.

$(\varepsilon_r + \delta_r) \beta \left(\left| \tilde{T}/2 \right| + \left| \varepsilon_z \tilde{E} - \tilde{T}/2 \right| \right)$, $(\varepsilon_r + \delta_r) \lambda \left| \tilde{T} \right|$, $\left| \tilde{E} \right| \varepsilon_r \delta_r$ increase the angle error far beyond values reported in [13]. The appearance of mixed error terms follows from the fact that the first order terms in the Taylor series expansion of the magnetic fields vanish due to the high symmetry of the arrangement. Thus the dominant errors are caused by second order terms which also include mixed error terms. In practice these mixed error terms are larger than the pure terms. Therefore they are responsible for the long tail in the distribution function, which was shown in [8, 9]: If the occurrence of a single large parameter of assembly tolerance is e.g., 1-in-1000 then the occurrence of a mixed error term is 1-in-1000000. Hence, the mixed error terms lead to the rare outliers of the distribution function of the angle error. The general conclusion is that a high degree of symmetry of magnetic sensor systems leads to small typical errors yet to large worst case errors. In other words, the symmetry of the sensor system has little effect on worst case samples, yet it greatly improves the typical sample.

6. ANGLE ERROR VERSUS SIZE OF MAGNET

With (23) it is straightforward to compute the worst case angle error for a given set of assembly tolerances and for various shapes of magnets. However, there are also some practical limitations, which we should bear in mind:

1. The thickness of the magnet in axial direction should not be too large. This keeps the demagnetization factor low and achieves strongest field with a minimum magnetic mass. Besides, slim magnets increase the contribution of higher order moments to the magnetic field. This is favourable for the angle error: As was shown in [8] a pure magnetic dipole has larger shape functions than flat disks.
2. For similar reasons the sensor should be as close to the magnet as possible: this emphasizes the influence of higher order multipole moments.
3. Magnets with small diameters should be avoided. Not only do they have larger shape functions, they also suffer from larger tilt errors due to their small top surface, which serves as reference plane during magnetization and assembly. Values of up to 5° for cheap magnets are quoted by some manufacturers. It may be necessary to fix the magnet to the shaft prior to magnetization.
4. The size of the magnet does not only influence the angle error via the shape functions, it also determines the strength of the

applied field. All types of sensors require a minimum field and some even require that the field does not become too strong. The strength of the field may also vary by about one decade due to the remanence of the magnet material. It is advisable to use large, cheap ferrites with small remanence instead of small, expensive rare-earth magnets with large remanence. In order to avoid deformation and shrinkage due to sintering, injection molded magnets are frequently used.

5. Cylindrical magnets have smaller shape functions than square magnets. Blocks of magnets with a long extension in the x - or y -direction have large shape functions [8].
6. The position tolerances of sensors in cheap packages can be significant: Typically the lateral position accuracy is between $100\ \mu\text{m}$ and $150\ \mu\text{m}$ and the tilt of the semiconductor die referred to the surface of the package may be up to 3° .
7. Total assembly tolerances of an angle sensor include (i) tolerances of the semiconductor die in the sensor package, (ii) tolerances of mounting the package to a board, (iii) tolerances of mounting the board to a chassis, (iii) tolerances of mounting the magnet to the shaft, (iv) static and dynamic tolerances of the shaft in the bearing. Moreover, these parameters may be subject to thermo- and hygro-mechanical strain and cure shrink of plastics over lifetime. Therefore the worst case tolerances in a cheap low-cost assembly line may be $\beta = 6^\circ$, $\lambda = 4.5^\circ$, $\varepsilon_r = 0.25\ \text{mm}$, $\delta_r = 0.25\ \text{mm}$.

Figure 5 shows the worst case angle error for various shapes and sizes of magnets. It is obvious that the angle error decreases drastically with the size of the magnet, yet, for large magnets it does not decrease beyond a certain limit of 0.72° , which is defined by the tilt angles β and λ in the homogeneous magnetic field of a large magnet. Cylindrical magnets have lower angle error than block shaped ones, nonetheless it is still 1.53° for 10 mm large magnets. Obviously 5 mm small blocks or cylindrical magnets may lead to severe angle errors of 3.5° . Note that all types of magneto-resistors (AMR and GMR) are subject to this error in spite of optimized layout according to (22). Also other types of magnetic angle sensors (e.g., vertical Hall effect sensors) suffer from this error, because it is caused by the projection of the magnetic field onto a misaligned sensor surface. However, the error can be kept sufficiently small by large enough magnets or optimized shapes of magnets, as discussed in Section 8.

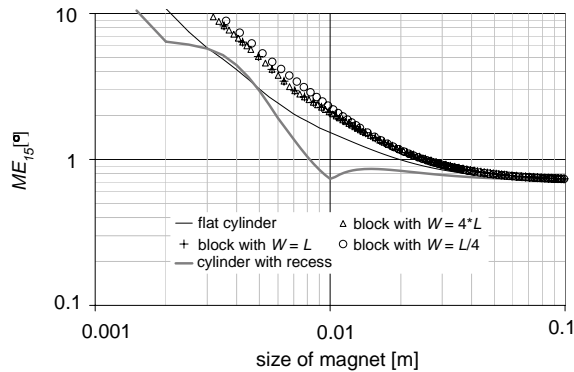


Figure 5. Worst case angle error ME_{15} versus size of magnet for various magnet geometries. The size is equal to the diameter for cylindrical magnets and it is equal to the length of the diagonal of the footprint for block shaped magnets. For block shaped magnets W denotes the width in x -direction and L is the length in y -direction. All magnets are polarized along the y -direction. In axial direction they are 2.5 mm thick. The distance of the sensor to the center of the magnet is 2.05 mm. Worst case assembly tolerances are $\beta = 6^\circ$, $\lambda = 4.5^\circ$, $\varepsilon_r = \delta_r = 0.25$ mm. The cylindrical magnet with recess is discussed in Section 8. For outer diameters around 10 mm its curve shows a marked dip. There it halves the angle error of flat cylindrical magnets and achieves the same values as in the limit of perfectly homogeneous fields of very large magnets.

7. THE MICRO-LINEARITY ML

For applications like motor control it is necessary to know how much the sensor reading differs if the mechanical angle varies only little around a quiescent point. If the sensor exhibits hysteresis or quantization this may result in comparatively large jumps in the sensor reading despite only tiny changes in the mechanical angle. Yet also assembly tolerances may lead to distortions so that the sensor readings do not vary by the same amount as the mechanical angle. To this end we define the micro-linearity as $ML = (\varphi'(\varphi + \phi) - \varphi'(\varphi))/\phi$ in the limit of vanishing ϕ . Here φ' is the apparent angle as defined in (5) and φ is the true angle of rotation. It follows $ML = 1 - \partial\Delta\varphi/\partial\varphi$. For $\Delta\varphi$ we may use (19)–(21). Thus the micro-linearity may be computed similarly to the angle error and similar terms show up there. For a worst case estimation we may add all ten amplitudes in this expression:

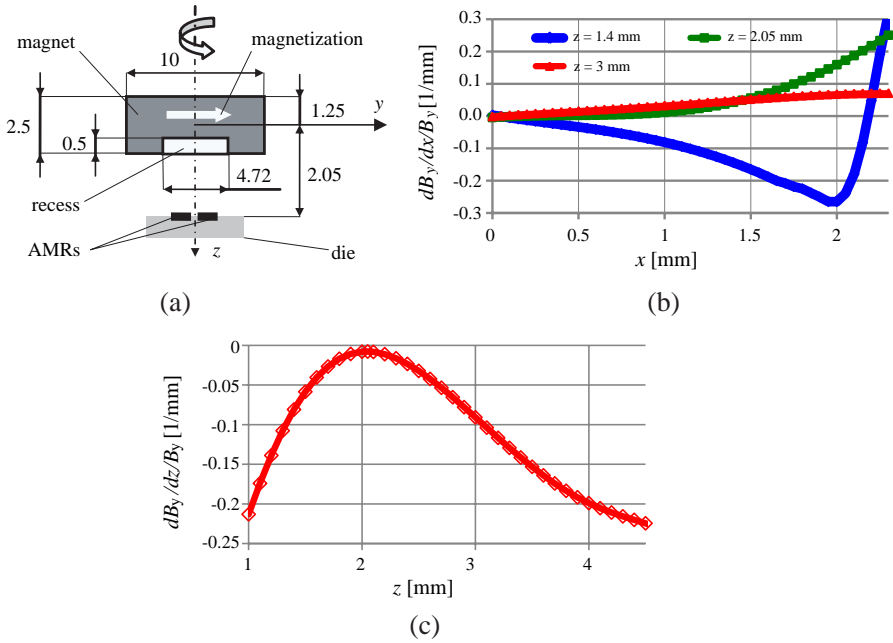


Figure 6. Optimized shape of cylindrical magnet with small recess. Lengths are given in millimeters. The eccentricity shape function vanishes at $z = 2.05$ mm (cf. Figure 6(b)) and the tilt shape function is very small there (1/212 mm, cf. Figure 6(c)). Field plots were obtained from finite-element simulation. (a) Dimensions of magnet and distance to sensor die. (b) Slope of $dB_y(x, 0, z)/dx$ versus x for $z = 1.4$ mm, 2.05 mm, and 3 mm. (c) $dB_y(0, 0, z)/dz$ versus z .

$ML = 1 \pm A \times MNL_{10}$ with

$$\begin{aligned}
 MNL_{10} = & \lambda^2/2 + \beta\lambda \left| 1 + \varepsilon_z \tilde{T} \right| + (\varepsilon_r + \delta_r) \left(\varepsilon_r \left| \tilde{E} \right| + \lambda \left| \tilde{T} \right| \right) \\
 & + \varepsilon_r \beta \left(\left| \tilde{T}/2 \right| + \left| \tilde{T}/2 - \varepsilon_z \tilde{E} \right| \right)
 \end{aligned} \quad (24)$$

with the worst case micro-nonlinearity MNL_{10} . Again the factor A is close to one as in Section 5. Typical values of MNL_{10} are around 0.3% for typical assembly tolerances and negligible hysteresis and quantization. MNL_{10} is a measure for local nonlinearity like the DNL (= differential non-linearity) is for analog-to-digital converters.

8. THE OPTIMUM MAGNET

Optimum magnets have vanishing shape functions $\tilde{E} = \tilde{T} = 0$. This is a less stringent requirement than forcing the applied magnetic field to

be perfectly homogeneous near the sensor elements, as is shown in the following.

Since the curl of the flux density vanishes everywhere we get $\partial \left(\vec{n}_z \cdot \left(\vec{\nabla} \times \vec{B} \right) \right) / \partial x = 0 \Rightarrow \partial^2 B_x / \partial x / \partial y = \partial^2 B_y / \partial x^2$. Thus, the eccentricity shape function \tilde{E} vanishes if the curvature of the B_y -field along the x -direction vanishes:

$$\tilde{E}(z) = \frac{1}{B_y(0,0,z)} \frac{\partial^2 B_y(0,0,z)}{\partial x^2}. \quad (25)$$

Similarly the vanishing curl of the flux density $\vec{n}_x \cdot \left(\vec{\nabla} \times \vec{B} \right) = 0 \Rightarrow \partial B_y / \partial z = \partial B_z / \partial y$ means that the tilt shape function \tilde{T} vanishes if the B_y -field has a flat plateau along the rotation axis:

$$\tilde{T}(z) = \frac{1}{B_y(0,0,z)} \frac{\partial B_y(0,0,z)}{\partial z}. \quad (26)$$

Equations (25) and (26) are particularly helpful if one uses numerical simulation tools to optimize the magnet. One simply has to investigate the B_y -field around the centre of the sensor along both directions perpendicular to the magnetization. This has been done for the optimized magnet in Figure 6(a). It has a small recess on the surface of the magnet, which faces the sensor. With this recess one makes both shape functions vanish, as is shown in Figures 6(b) and 6(c). This leads to angle errors, which are only half as big as the errors of simple cylinders (cf. Figure 5).

9. CONCLUSION

Assembly tolerances lead to significant errors of magnetic angle sensors. It was shown that AMR sensors have similar angle errors to GMR sensors. In both cases parts of these errors can be eliminated by optimized layouts according to (22). However, for both types of sensors it is more effective to use optimized magnets with vanishing shape functions (25) and (26). For the first time an example of such an optimized magnet was given (cf. Section 8). Also for the first time an approximate value for the angle error caused by worst case combinations of assembly tolerances was given (cf. (23)). These findings are valuable for the design of robust XMR angle sensors that are mass produced in standard industrial assembly lines.

REFERENCES

1. Granig, W., S. Hartmann, and B. Koepl, "Performance and technology comparison of GMR versus commonly used angle sensor principles for automotive applications," *SAE World Congress & Exhibition*, Detroit, USA, April 2007.
2. Wegelin, F., "Eine neue generation magnetoresistiver sensoren fuer das automobil," Vortraege der 15. ITG/GMA-Fachtagung, Nuernberg, Germany, May 18–19, 2010.
3. Tumanski, S., *Thin Film Magnetoresistive Sensors*, IOP Publishing, Bristol, Philadelphia, 2001, ISBN 0750307021.
4. Andreev, S. and P. Dimitrova, "Anisotropic-magnetoresistance integrated sensors," *J. Optoelec. Advanced Materials*, Vol. 7, No. 1, 199–206, 2005.
5. Dietmayer, K., "Magnetic sensors on the AMR-effect," *TM — Technisches Messen*, Vol. 68, No. 6, 269, 2001.
6. Adelerhof, D. J. and W. Geven, "New position detectors based on AMR sensors," *Sens. Actuators A*, Vol. 85, Nos. 1–3, 48–53, 2000.
7. Dietmayer, K., "Integrated online diagnosis for AMR-based angular measurement systems," *Sens. Actuators A*, Vol. 91, Nos. 1–2, 12–15, 2001.
8. Ausserlechner, U., "Inaccuracies of giant magneto-resistive angle sensors due to assembly tolerances," *IEEE Trans. Magn.*, Vol. 45, No. 5, 2165–2174, 2009.
9. Ausserlechner, U., "The optimum layout for giant magneto-resistive angle sensors," *IEEE Sensors Journal*, Vol. 10, No. 10, 1571–1582, 2010.
10. Arfken, G., *Mathematical Methods for Physicists*, 3rd Edition, 198–200, San Diego, Academic, CA, 1985.
11. http://cms.hlplanar.de/data-live-planar/docs/pdf/Datasheets_USA/MEAS_MR.pdf.
12. Hastings, A., *The Art of Analog Layout*, 231, Prentice Hall, Englewood Cliffs, NJ, 2001.
13. Kolbe, N. and M. Prochaska, "Ueber den einsatz von hochintegrierten magnetfeldsensoren im antriebsstrang," Paper 9, 42–46, *Automotive Meets Electronics*, Dortmund, Germany, April 15–16, 2010, ISBN 978-3-8007-3236-4, VDE VERLAG GMBH Berlin Ofenbach.